Available online at www.sciencedirect.com
ScienceDirect
Earth and Planetary Science Letters 261 (2007) 20–32
EPSL
www.elsevier.com/locate/epsl

Conditions for the onset of plate tectonics on terrestrial planets and moons

C. O'Neill [a,*], A.M. Jellinek [b], A. Lenardic [a]

[a] Department of Earth Sciences, Rice University, Houston, Texas, 77005, USA
[b] Department of Earth & Ocean Sciences, University of British Columbia, Vancouver, BC, Canada

Received 31 May 2006; received in revised form 22 February 2007; accepted 20 May 2007
Available online 26 May 2007
Editor: C.P. Jaupart

Abstract

Plate tectonics on Earth is driven by the subduction and stirring of dense oceanic lithosphere into the underlying mantle. For such a regime to exist on any planet, stresses associated with mantle convection must exceed the strength of the lithosphere. This condition is sufficiently restrictive that plate tectonics currently operates only on Earth, and mantle convection in most terrestrial planets and moons is probably in a stagnant lid regime. Convective stresses on the lithosphere depend on the viscosity and velocity of underlying cold downwellings. The lithospheric yield stress is controlled by its friction coefficient and elastic thickness (the depth to the brittle–ductile transition or BDT). Both convective stresses and the plate's yield strength depend critically on the size, thermal state and cooling history of a planet. Accordingly, here we use numerical simulations and scaling theory to identify conditions in which mantle convection leads to lithospheric failure for a range of conditions relevant to the terrestrial planets. Whereas Earth is expected to be in a plate-tectonic regime over its full thermal evolution, the Moon and Mercury are expected to have always remained in a stagnant lid regime. Venus, Io and Europa currently fall on the transition between the two regimes, which is consistent with an episodic style of mantle convection for Venus, a tectonic component to deformation on Io, and the resurfacing history and lithospheric evolution of Europa. Our results suggest that Venus may have been in a plate-tectonic regime in the past. While stagnant now, it is plausible that Mars may have also been in an active-lid regime, depending on whether there was liquid water on the surface.

Keywords: mantle convection; plate tectonics; lithosphere; terrestial planets

1. Introduction

Mantle convection is thought to occur in two end-member regimes (Moresi and Solomatov, 1998). The plate-tectonic regime on Earth is an example of "active-lid" convection, involving the foundering and stirring of cold lithosphere into the underlying mantle (Moresi and Solomatov, 1998; Solomatov, 2004a,b). The recycling of the upper "lid" – irrespective of the detailed mechanism – has important consequences for the thermal structure of the mantle, and lid resurfacing may have been important for other terrestrial bodies in their recent evolution (Turcotte, 1993; McKinnon et al., 2000). The style of flow inferred for most terrestrial

* Corresponding author. Now at GEMOC ARC National Key Centre, Department of earth and Planetary Science, Macquarie University, NSW, Australia, 2109.
E-mail addresses: coneill@els.mq.edu.au (C. O'Neill), mjellinek@eos.ubc.ca (A.M. Jellinek), adrian@geophysics.rice.edu (A. Lenardic).

0012-821X/$ - see front matter © 2007 Published by Elsevier B.V.
doi:10.1016/j.epsl.2007.05.038

planets and moons, however, is the "stagnant lid" regime in which mantle convection occurs beneath a strong, intact, and immobile lithosphere (Ogawa et al., 1991; Moresi and Solomatov, 1995; Solomatov and Moresi, 1997; Solomatov and Moresi, 2000). This regime is a consequence of the strong temperature-dependence of the mantle viscosity and arises because the coldest upper part of the lithosphere is too viscous to take part in the underlying flow (Ogawa et al., 1991; Solomatov and Moresi, 2000), and the yield strength of the viscous lid is too high to permit brittle failure. Motion is expected to take the form of intermittent discrete thermals sinking from beneath the lithospheric lid and rising from the core–mantle boundary (Manga et al., 2001; Jellinek et al., 2002; Jellinek and Manga, 2004). Moresi and Solomatov (1998) also delineated an intermediate regime between these two extremes where convection takes the form of catastrophic lid overturns, followed by longer periods of surface quiescence — essentially an oscillation between the active and stagnant modes. They found that a planet's tectonic regime depends critically on the ratio of lithospheric strength to natural convective stresses: if the stresses imposed by convection exceed the lithospheric strength, the lithosphere will founder, if not, the lithosphere will remain intact in a stagnant-lid mode.

Whether a planet that is initially in a stagnant lid regime can enter a plate-tectonic regime depends on whether viscous stresses arising due to the formation of sinking thermals exceed the intrinsic strength of the lithosphere, which depends on temperature, water content and applied stress. The question we pose is under what conditions are such convective stresses sufficient to initiate subduction? It should be stressed that breaking a plate is not in itself the sole criterion for a plate-tectonic style of flow, though it is a necessary one. In posing this question we implicitly assume an oceanic rheology for Earth, and a similarly simplified rheology for other planets. We ignore chemical variations and surface heterogeneities, and also ignore complexities essential to realistic modelling of plate tectonics such as weakening mechanisms, ductile localization etc. We specifically address the problem of the effective strength of the lithosphere on different planets, and what conditions are necessary to break it.

In the simplest model for plate failure, a plate may permanently deform by two mechanisms; brittle failure in the cool shallow regions of the lithosphere, or by viscous flow in the hotter, deeper regions (Fig. 1). The maximum supportable lithospheric stress generally occurs at the intersection of these two regimes, ie. the brittle–ductile or brittle–plastic transition (Kohlstedt et al., 1995). Compositional heterogeneities or alternative deformational mechanisms (such as plastic flow) can complicate this simple conceptual model, but it remains a sensible estimate for effective lithospheric strength. Maggi et al. (2000) demonstrate that the depth to which seismicity, and, by inference, brittle behaviour occurs also corresponds to the elastic lithospheric thickness. The elastic lithospheric thickness is controlled by the temperature at which significant stress-relaxation occurs over geological times; ~450 °C from flexural studies on oceanic lithosphere (Calmant et al., 1990; Turcotte and Schubert, 2002; Watts and Burov, 2003), but higher for dry rheologies — and thus will scale with the thermal boundary layer (ie. lid) thickness. Assuming Byerlee's frictional law (Byerlee, 1968), the maximum stress that can be accommodated without deformation

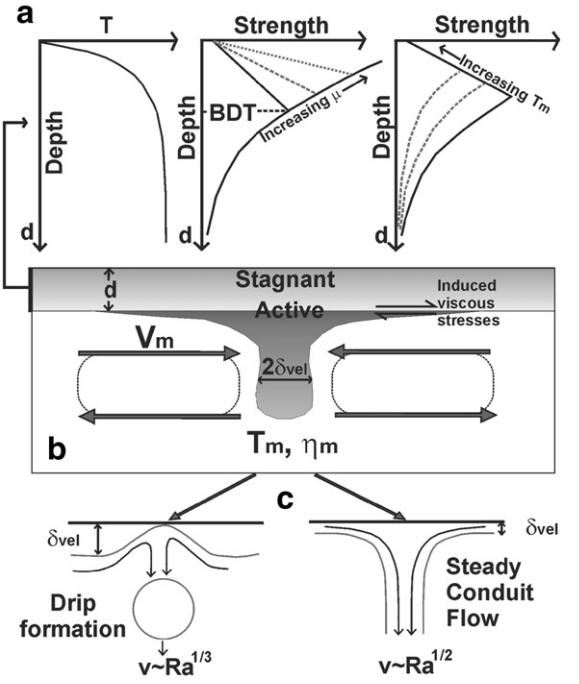

Fig. 1. (a) Deformation mechanisms within a cold lid with a viscoelastic–plastic rheology. The lid behaves elastically at low stress and temperature (T), ie. above the BDT, and viscously below the BDT. The lid fails and behaves in a brittle manner once lithospheric stresses exceed the yield stress. Dashed lines show the qualitative effect of increasing the friction coefficient μ (middle) and increasing temperature (right). (b) Experimental setup for our numerical simulations. We impose a strong lid of thickness d. The mantle beneath the lid is at a constant T_m, with a viscosity η_m, and is stirred by two conveyor belts (shown by horizontal arrows) turning at a velocity V_m, which we vary. The convective stress imparted on the lid is a function of the velocity of the active downwelling (centre), generally V_m in our simulations. (c) Sub-lithospheric velocities due to cold-downwellings, either in the form of a sinking drip (left) or steady flow into a conduit (right Worster and Leitch, 1985).

is proportional to elastic thickness. Fig. 1 highlights two variables which affect the BDT, the coefficient of friction μ, and the temperatures at the base of the lithosphere. Dry rock experiments (Byerlee, 1968) constrain the value of μ to be 0.6–0.85, depending on pressure, which we adopt for most planets. However, modelled deformation on Earth (Beaumont et al., 2000), and experiments on serpentinized rocks (Escartin et al., 1997; Escartin et al., 2001), and computer simulations of fault strength (Bird and Kong, 1994) suggest a much lower coefficient of friction ($\sim$0.15) for planets with liquid water on the surface (ie. Earth and maybe early Mars). The effective friction coefficient for cold ice is taken to be 0.6 (Beeman et al., 1988). Bearing in mind the complications involved in defining the BDT explicitly, for given temperature-stress-water content conditions it is appropriate to define an analog lithosphere constructed of two mechanical components: Above the BDT is the stagnant lid or "plate" component, which behaves in an essentially elastic way over the time scales for convection. Below the BDT is the "viscous" part of the cold boundary layer — which forms the strong core of the lithosphere, though the lower parts (the rheological boundary layer) will participate in mantle convection.

Previous work by Solomatov (2004a,b) has shown that the convective stresses for an Earth-like planet require a low lithospheric yield strength ($\sim$3 MPa) to initiate subduction (Solomatov, 2004b). This value is fairly low value for lithospheric yield strength; in comparison, Kohlstedt et al. (1995) show yield strength envelopes for dry olivine capable of supporting $\sim$500 MPa, and Kanamori (1994) shows that stress drops during earthquakes (the minimum the lithosphere is supporting) to be typically in the range of 3–10 MPa. High stress drops during some earthquakes may be up to 250 MPa (Kanamori, 1994). Possible factors in Solomatov's (2004a,b) low yield strength estimate include a large lid-convecting layer thickness ratio, affecting the stress coupling between convective features and the lithosphere; the *a priori* assumption of a 100 km lithospheric thickness in applying the scalings to terrestrial planets; and the assumption that the plastic zone extends to 0.5 the depth of the lid (Solomatov, 2004a).

With these limitations in mind, we build on the work of Solomatov (2004a) in three ways. First, to improve understanding of the stress regime associated with individual drips we use a forced convection setup, in which the drip velocity and convective stress is specified *a priori*, to map conditions leading to either an intact or failed lithosphere. Results are then applied to mantle convection using well-established scalings for convective velocity and stress. The condition for intact or failed lithosphere is verified by a scaling theory that follows (Solomatov, 2004a). Second, we assume that the thickness of the brittle lithosphere (or the elastic thickness) will scale with the cold thermal boundary layer thickness and consequently let the lithospheric yield condition be determined by the heat transfer properties of the convecting system, as well as the choice of effective friction coefficient. Third, by casting the driving convective stress, retarding lithospheric yield stress and the condition for lithospheric failure in terms of an appropriate Rayleigh number for mantle convection we are able to map the evolution of such conditions as a function of the thermal history of a planet. We explore the evolution in tectonic regime for the terrestrial planets and a number of Jovian moons.

2. Theory

2.1. Driving forces

Stagnant lid convection takes the form of drips from the viscous region of the lower lithosphere. This viscously deforming regions constitutes the "rheological" boundary layer defined by Reese et al. (1998), ie. the active part of the thermal boundary layer. The thickness of this layer depends on the thermal contrast across the boundary layer, and the viscosity law. Mantle viscosities are strongly temperature dependent, and follow an Arrhenius flow law, but a good approximation to this behaviour is the Frank–Kamenetski approximation (Reese et al., 1998), which takes the form:

$$\eta_{\mathrm{lid}} = \frac{b}{\tau^{n-1}} e^{-\gamma T} \tag{1}$$

where $n=1$ corresponds to a Newtonian fluid, $n>1$ is for a power-law rheology, and b and γ are constants (Solomatov, 2004a; Batchelor, 1954), τ the stress and T the temperature. γ is related to the total system viscosity contrast $\Delta\eta$ by $\ln(\Delta\eta)(=\theta)=\frac{\rho H d^2}{k\gamma^{-1}}$, where ρ is the density, k is the thermal conductivity, H is the internal heat production rate, and d is the convective depth scale. We assume $\Delta\eta$ is 10^5 for all our simulations with normalised temperatures of $\Delta T=1$. Thus at low temperatures, the lid is extremely viscous, and effectively removed from participating in mantle convection. Lower in the lid, though, higher temperatures enable the mobility of the rheological boundary layer, resulting in the periodic formation of drips which descend into the mantle.

Flow into these drips imparts a viscous stress to the base of the stagnant lid, which scales as

$$\tau_{xz} = \frac{v_x \eta}{\delta_{\mathrm{vel}}} \tag{2}$$

where τ is the stress, v is a velocity scale that we discuss below, η is the viscosity of the active, viscously deforming lithosphere, δ_{vel} the velocity boundary layer thickness (Turcotte and Schubert, 2002) (Fig. 1), and x and z subscripts denote horizontal and vertical directions respectively. Examination of Eq. (2) indicates that for a given convective regime the viscous stress imparted to the lithosphere by flow into nascent drips depends critically on the velocity of the flow and the viscosity of the rheological sublayer.

2.2. Plate resistance

A plate permanently deforms by either brittle failure and viscous flow. The criteria for yielding is defined by Byerlees' law (Byerlee, 1968) $\tau_{\mathrm{yield}} = C_0 + \mu P$, where C_0 is the cohesion, μ is the coefficient of friction, and P is the pressure. Brittle failure is the dominant failure mechanism in the cold, near surface portions of the plate. We model plate failure by using an effective viscosity once the material's total deviatoric stress exceeds the yield stress. This effective viscosity is defined by τ_{yield}/D (where D is the second invariant of the strain rate tensor). In the deeper portions of the lithosphere, viscous flow is the dominant deformation mechanism, assuming the flow law described in Eq. (1).

Below the yield stress, the lithosphere may deform elastically. Though this does not directly affect the yield stress, elasticity may affect the distribution of stress within a plate, potentially focussing stress at some depths, affecting our scaling relationships. Our simulations are geometrically consistent, so elastic effects are similar in all cases, and implicitly included in our geometric scaling prefactors. They are also second-order to applied stresses, as demonstrated in Appendix B.

The maximum supportable lithospheric stress occurs at the brittle–ductile transition (BDT), ie. the intersection of the brittle and viscous deformational styles. The depth of this transition depends on both the coefficient of friction μ and the mantle temperature T_{m}. This simple conceptualization is of course more complicated for composite, layered rheologies (Kohlstedt et al., 1995). However, on Earth, most regions of complicated rheology (ie. continents) are generally buoyant and resistant to subduction. Both viscoelastic–plastic rheology and Byerlee's law appear to be reasonable first approximations to the rheology and yield stress of the oceanic lithosphere. Indeed, analyses of the dynamics of diffuse oceanic boundaries (Gordon, 2000) suggest that the depth-integrated rheology of the oceanic lithosphere is characterized by Eq. (1) where $n \sim 6$, which is quantitatively similar to a plastic rheology (Jellinek et al., 2006).

2.3. Lid failure and planetary evolution

Whether buoyancy-driven viscous stresses can generate failure of the lithosphere depends strongly on the thermal state of the planet. Thus, such a condition may be understood in terms of the variation in Rayleigh number through time. As noted by Moresi and Solomatov (1995) the upper immobile portions of the lid have little influence on interior convection, and it is more useful to define the Rayleigh number as:

$$Ra_{\mathrm{rh}} = \frac{g\rho\alpha\Delta T_{\mathrm{rh}} d^3}{\kappa \eta_{\mathrm{rh}}}. \tag{3}$$

Here ρ is the density, α is the thermal expansivity, g is the acceleration due to gravity, d is the depth of the convecting mantle, and κ is the thermal diffusivity (see Table 2 for values). The subscript rh refers to the rheologically active part of the lithosphere, where η_{rh} is the average layer viscosity, and ΔT_{rh} is the temperature drop across this layer.

Our goal is to derive scalings for an easily observed planetary parameter – the elastic lithospheric thickness (T_{e}, equivalent to the brittle–ductile transition (Maggi et al., 2000)) – which is an isotherm and thus some fraction of the TBL thickness, and the driving terms such as velocity. Solomatov and Moresi (2000) show that velocity and thermal boundary layer thickness scale as $v = A(\kappa/d_{\mathrm{mantle}})\ (Ra/\theta)^{\beta}$, and $\delta = (d_{\mathrm{mantle}}/B)(\theta^{\alpha}/Ra^{\lambda})$ respectively. Here A and B are constants, $\theta = \ln(\Delta\eta)$, $\Delta\eta$ is the viscosity contrast, and the exponents α, β and λ depend on the dynamics of the problem and specific rheology, and are given in Table 1 for a number of scenarios. Substituting these terms into Eq. (2) yields an expression for the convective stress:

$$\tau_{c,xz} = AB\frac{\eta\kappa}{d_{\mathrm{mantle}}^2}\frac{Ra_{\mathrm{rh}}^{\beta+\lambda}}{\theta^{\beta+\alpha}}. \tag{4}$$

The maximum supportable stress for any depth will occur at the intersection of the brittle and ductile regimes (ie. at d_{BDT}), and can be expressed as $\tau_{\mathrm{r}} = \mu\rho g d_{\mathrm{BDT}}$. Since the depth to d_{BDT} is a temperature isotherm, this can be re-written as $\tau_{\mathrm{r}} = \mu\rho g(c\delta)$ where c is a constant

Table 1
Relevant scaling coefficients

Case	n	α	$\beta 1$	$\beta 2$	λ
Drip formation	1	4/3	1/3 [a]	–	1/3
Steady pipe flow	1	4/3	1/2 [b]	–	1/3
RMS interior	1	4/3	2/3	1/2	1/3
RMS interior	3	8/5	6/5	21/20	3/5
Forced convection [c]	1	4/3	2/3	–	–

Here, $\alpha=2(n+1)/(n+2)$, $\beta 1=2n/(n+1)$ [d], $\beta 2=(2n+1)/(n+1)(n+2)$ [e, f], $\lambda=n/(n+2)$ [f].

[a] β determined for Stoke's flow.

[b] Kaminski and Jaupart (2003) — β determined experimentally.

[c] We pre-define the velocity conditions, thus the velocity boundary layer thickness does not vary with convective vigor in the forced convection case.

[d] Reese et al. (1998) — assuming dissipation occurs throughout mantle.

[e] Solomatov and Moresi (2000) assuming all dissipation occurs in the active part of the lid.

[f] Solomatov (2004a).

between 0 and 1, and δ is the thermal boundary layer thickness. Now if we also assume the velocity boundary layer is some fraction of the TBL thickness ($f\delta$, $0<f<1$), then equating τ_r and τ_c gives

$$\begin{aligned}
&\mu\rho g(c\delta)\approx\left(\frac{\nu\eta}{\delta_v}\right)\approx\frac{A(\kappa/d_{\mathrm{mantle}})(Ra/\theta)^{\beta}\eta}{(f\delta)}\\
&\left(\frac{1}{d_{\mathrm{mantle}}}\right)^2(c\delta)^2=\left(\frac{1}{d_{\mathrm{mantle}}}\right)^2\frac{Ac}{f}\frac{\eta\kappa}{\mu\rho g}\frac{1}{d_{\mathrm{mantle}}}\left(\frac{Ra}{\theta}\right)^{\beta}\\
&\frac{d_{\mathrm{BDT}}}{d_{\mathrm{mantle}}}\approx E\left(\frac{\eta\kappa}{\mu\rho g}\right)^{\frac{1}{2}}\left(\frac{1}{d_{\mathrm{mantle}}}\right)^{3/2}\frac{Ra^{\beta/2}}{\theta^{\beta/2}}.
\end{aligned}\tag{5}$$

Here we have combined a number of constants into the constant E. For the simplest definition of $\beta=(2n/(n+2))$ (Table 1), assuming dissipation occurs throughout the mantle, and that $n=1$, then $\beta=2/3$. Note that for driven convection, where we impose velocity conditions (Fig. 1), we have implicitly imposed the velocity boundary layer thickness, and thus the convective stress scales as $\tau_c\sim Ra^{2/3}$. Subsequently the transition between intact and failed lithosphere (Eq. (5)) will scale as $Ra\sim(d_{\mathrm{BDT}}/d_{\mathrm{mantle}})^3$. Alternatively, from Eq. (5), we can see that equating τ_r and τ_c results a dependency on δ on both sides. Grouping these together, we can define a "driving motive" $F_{\mathrm{drive}}=v\eta$, which, while not dimensionally a force or stress, encapsulates all the important driving terms for the system. The motivation for expressing the driving terms in such a manner is that it allows us to plot them against the depth to the brittle–ductile transition, or T_e, in an obvious manner. Its relation to d_{BDT} is given by $F_{\mathrm{drive}}\sim(d_{\mathrm{BDT}}/d_{\mathrm{mantle}})^2$.

For the formation of a Newtonian sublithospheric drip the relevant exponents are $\beta=\lambda=1/3$. In this case, while the convective stress scales similarly, ($\tau_c\sim Ra^{2/3}$), the transition (Eq. (5)) will scale as $Ra\sim(d_{\mathrm{BDT}}/d_{\mathrm{mantle}})^6$. Another appropriate scaling for the sublithospheric velocity is that for a steady laminar downwelling ($\beta=1/2$) (Batchelor, 1954; Worster and Leitch, 1985; Kaminski and Jaupart, 2003; Solomatov, 2004a). Alternatively, we note that the rheology of the viscous region may be stress dependent and better described by a non-Newtonian power law such that $\varepsilon\sim\tau^n$, where $n\approx 3$ (Reese et al., 1998). In general the effect of including such a power-law rheology is to enhance the relative velocity of downwelling drips, and hence our results are conservative in their estimate of sublithospheric velocity and driving force. A lower bound on the velocity and viscous stress for the $n=3$ case is an RMS mantle velocity derived numerically (Reese et al., 1998) ($\beta=1.21$). Additionally, if the velocity boundary layer thickness is not simply related to thermal boundary layer thickness, then Eqs. (4) and (5) break down (ie. the relation $\delta_{\mathrm{velocity}}=f\delta_{\mathrm{thermal}}$ does not hold). This might be the case for high Rayleigh numbers with significant internal dissipation (Reese et al., 1998). Clearly there are complexities in these scaling relationships, and have sought to incorporate the ambiguities of different exponents in our uncertainties. For the most part, though, we will consider the case of sublithospheric drip formation in calculating relevant velocities and driving stresses for the planets.

3. Numerical model description

In order to simulate the scenario in Fig. 1, we employ a particle-in-cell finite element code (Ellipsis (Moresi et al., 2003)). We solve the standard convective equations for momentum and energy subject to the incompressibility constraint. The momentum equation can be written as

$$\begin{aligned}
&\nabla\cdot\sigma=\mathbf{g}\rho_0\alpha T\\
&\sigma_{ij}=2\eta D_{ij}-p\delta_{ij}.
\end{aligned}\tag{6}$$

Here η is the viscosity, $D_{ij}=(\partial v/\partial x_j+\partial v_j/\partial x_i)/2$ is the rate of deformation tensor, p is the dynamic pressure, ρ_0 is the reference density, $\mathbf{g}$ is the gravitational acceleration, α is the thermal expansivity, and T is the temperature. Flow is subject to the incompressibility constraint:

$$\nabla\cdot v=0.\tag{7}$$

And the energy equation can be written as:

$$\frac{DT}{Dt}=\kappa\nabla^2T+Q.\tag{8}$$

Table 2
Physical properties and determined parameters for a number of terrestrial planets and icy moons

Planet/satellite	Depth of mantle (km)[a]	g (m/s^2)[b]	Ra[c]	Velocity (cm/yr)[d]	BDT (km)	Reference
Mercury	618	3.78	4.70E+04	0.130	70+/−40	(Siegfried and Solomon, 1974; Melosh, 1977)
Venus	2745	8.9271	1.92E+08	0.468	60+20/−40	(Smrekar and Stofan, 2003)[e]
Earth	2890	9.81	2.73E+08	1.000	40+/−20	(Schubert et al., 2001; Watts and Burov, 2003)
Moon	1340	1.62	9.66E+05	0.164	100+/−50	(Konopliv et al., 1998; Aoshima and Namiki, 2001)
Mars	1698	3.7278	7.26E+06	0.254	80+80/−60	(Folkner et al., 1997; McGovern et al., 2002)
Io	835	1.80	–	0.151	20+/−5	(Segatz et al., 1988; McKinnon et al., 2000)
Europa	170	1.32	–	0.631	6+5/−2	(Anderson et al., 1998; Nimmo et al., 2003)[f]
Ganymede	800	1.44	–	3.15E−6	1.3+/−0.4	(Anderson et al., 1996; Nimmo et al., 2002)[f]

[a] Determined by moment of inertia measurements on most planets to be the thickness of the convecting rocky mantle (for terrestrial bodies) or the thickness of the water ice/mush layer (for the Galilean icy satellites).

[b] From Table 14.1 of Schubert et al. (2001).

[c] Rayleigh number for a rheologically active "sublayer", $Ra = \frac{\rho\alpha g \Delta T_{\mathrm{rh}} d^3}{\kappa \eta_{\mathrm{rh}}}$, where ρ is the density (3400 kg/m^3), α is the thermal expansivity (3×10^{-5}), g is the acceleration due to gravity, d is the depth of the convecting mantle, and κ is the thermal diffusivity (10^{-6}). The subscript rh refers to the rheologically active part of the lithosphere, where η_{rh} is the average layer viscosity (assumed to be 5×10^{20} Pas — see (Tozer, 1972) for discussion of variability), and ΔT_{rh} is the temperature drop across this layer: $\Delta T_{\mathrm{rh}} = \Delta T\,\theta^{-1}$ (Reese et al., 1998), where ΔT is the system temperature scale $\frac{\rho H d^2}{k}$ for an internally heated system (Solomatov, 2004a), and $\theta = \ln(\Delta\eta)$ where $\Delta\eta$ is the viscosity drop across the system. Plausible viscosity contrasts are obtained for Earth when $\theta = 12$, and we use this value for all planets (nb. this is equivalent to $\gamma \sim 6e{-}3$ and an activation energy of ~200 kJ/mol for Earth-like parameters). Other parameters are k, the thermal conductivity (3), H the internal heating rate (assumed to be 7.4×10^{-12} W/kg at present for all terrestrial bodies, and 3.410^{-11} W/kg at 4.55 Ga based on the decay of ^{232}Th, ^{238}U, ^{235}U, and ^{40}K (Turcotte and Schubert, 2002). We have not determined Ra for the tidally heated Jovian satellites.

[d] Determined for the terrestrial planets using $v \sim Ra^{1/3}$, dimensionalized, and then other scaling constants are determined assuming a present day convection velocity of 1 cm/yr for Earth, and converted to stagnant lid velocities assuming $v_{\mathrm{stag}} \approx v_{\mathrm{mobile}}(Ra_{\mathrm{stag}}/Ra_{\mathrm{mobile}})^{1/3}$. Ra_{mobile} is for a conventional Ra with $\Delta T = 1400$ K and $\eta = 10^{20}$ Pas. Estimates for Io are based on resurfacing rate, and for Europa and Ganymede on independent estimates of strain rate (ie. calculating displacement vectors and average velocities per time interval assuming constant displacement rates). Note that the BDT for Europa and Ganymede are estimated from the elastic thickness of their ice shells.

[e] Depth of mantle assumed similar to Earth, scaled to Venus's smaller radius.

[f] Assuming convecting layer is the ice/ice-mush shell.

Here D/Dt is the material time derivative (taken at a point moving with respect to the fluid), κ is the thermal diffusivity, and Q is the volumetric heat production. The viscous flow law and brittle behaviour are described in Section 2, and their implementation previously described (Moresi and Solomatov, 1998; Reese et al., 1998). The Maxwell visco-elastic formulation is described in Moresi et al. (2003), and more fully outlined in Appendix A. The simulations are non-dimensionalized in the manner of Moresi and Solomatov (1998), assuming appropriate distance (d_0), viscosity (η_0), temperature (ΔT) and velocity (κ/d_0) scales (subscript 0 denotes reference value — see Table 2).

Our model is configured as follows (Fig. 1). The top and bottom conditions are free slip and constant temperature, and the side boundary conditions reflective. We perform our simulations in a 2×1 box using 254×128 nodes. Our analog plate is rigid with a viscoelastic–plastic rheology and a thickness and friction coefficient that we vary. The viscosity of the plate is temperature-dependent (Eq. (1)) with a total viscosity contrast of 10^5 — which, with the other system parameters effectively sets an activation energy. The plate overlies a convecting mantle with a prescribed temperature, constant viscosity, flow geometry and velocity, V_{m} (Fig. 1). Our imposed velocities (V_{m}) (arrows in Fig. 1) are set at a position of 0.1 units below the viscoplastic lid, 0.1 above the lower boundary, and range from 0.1 to 0.9 units (left hand side), and 1.1 to 1.9 units (right hand side). Their magnitudes vary (0–1000 in non-dimensional units), and are incorporated into the F_{drive} term. This forced convection problem setup enables us to apply a well-defined viscous stress to the base of the plate such that we can map the conditions leading to the stability or failure of the plate in a straightforward way and over a wide range of conditions. The brittle–ductile transition (BDT) is dependent on the imposed strain rate and thus imposed velocities, and we calculate it from the first timestep of the simulation, so it is self-consistent with the imposed velocities.

We perform an extensive series of simulations in which we vary the friction coefficient (ranges from 0.01 to 0.9), the temperature at the base of the lithosphere (0–1000 non-dimensional units (ndu)), velocity (0–1000 ndu), and mantle viscosity (0.01–500 ndu). Examples of plate stability and failure are shown in Fig. 2.

4. Results

Fig. 3a shows the variation in the normalised driving stress, F_{drive}/μ, against the normalised depth to the brittle–ductile transition, which is a proxy for the retarding yield stress of the plate for our suite of simulations. We identify a change in regimes, from intact to failed lithosphere, with increasing driving force or decreasing depth to the brittle–ductile transition. The dotted line demarks the division between failed and intact regimes predicted in Section 2.1 ($F_{\mathrm{drive}} \sim (d_{\mathrm{BDT}}/d_{\mathrm{mantle}})^2$) — where the convective stresses are sufficient to overcome a plate's intrinsic strength. The symbols are the results from our numerical models, for varying conditions appropriate to the terrestrial planets. Our scaling theory predicts the transition from failed to intact lithosphere extremely well over the range of parameters considered. Fig. 3b shows the same modelling results on a log–log graph, where we have recast the results assuming a $\mathrm{v} \sim Ra^{1/3}$ scaling, consistent with the formation of drips (Section 2.1, Fig. 1).

In Fig. 4 we have again plotted the normalised driving viscous stress against the depth to the brittle–ductile transition, on a log-linear scale. The dotted again demarks the transition from failed to intact lithosphere predicted by our theory. Here we have included the positions of the terrestrial planets and moons, based on the values listed in Table 2. We first calculated the Rayleigh number for the terrestrial planets based on the temperature drop across the rheologically active sublayer. The physical properties used are listed in Table 2. We assumed similar mantle heat production values to Earth, and similar viscosities in the active rheological sub-layer (5×10^{20} Pas, see Table 2). Assuming a typical mantle velocity of 1 cm/yr for Earth, we then use the relationship using $v \sim Ra^{1/3}$, subject to the modification for stagnant lid convection $v_{\mathrm{stag}} \approx v_{\mathrm{mobile}} (Ra_{\mathrm{stag}}/Ra_{\mathrm{mobile}})^{1/3}$(see Table 2). Rayleigh numbers and velocities were not estimated for the Jovian satellites, instead estimates for Io are based on resurfacing rate, and for Europa and Ganymede on independent estimates of strain rate. We non-dimensionalized these interior velocities, the viscosity of rheological sublayer (assumed

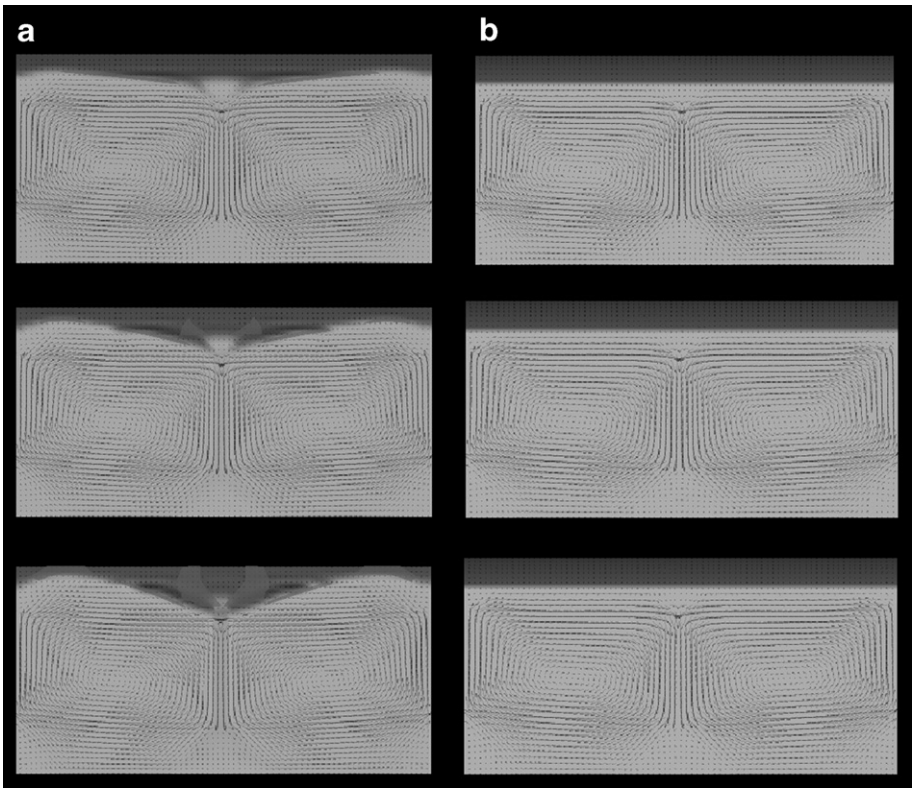

Fig. 2. Numerical simulation of failing lithosphere (a, left) and stable lithosphere (b, right). The viscoelastic–plastic lid overlies a viscous mantle. Areas undergoing plastic deformation are darkly shaded, and the velocity field is shown as arrows. All our simulations were performed using Ellipsis (see Moresi et al. (2003) for details) for the experimental setup shown in Fig. 1. Results are non-dimensionalized. The initial depth to the BDT in both cases is 0.08, and the coefficient of friction μ is 0.2. Both examples use a mantle viscosity of 1, a T_{m} of 100, and a lid thickness of 0.12. The imposed velocity (V_{m}) in (a) is 200, while for (b) its 10. The larger driving force in (a), results in lid failure.

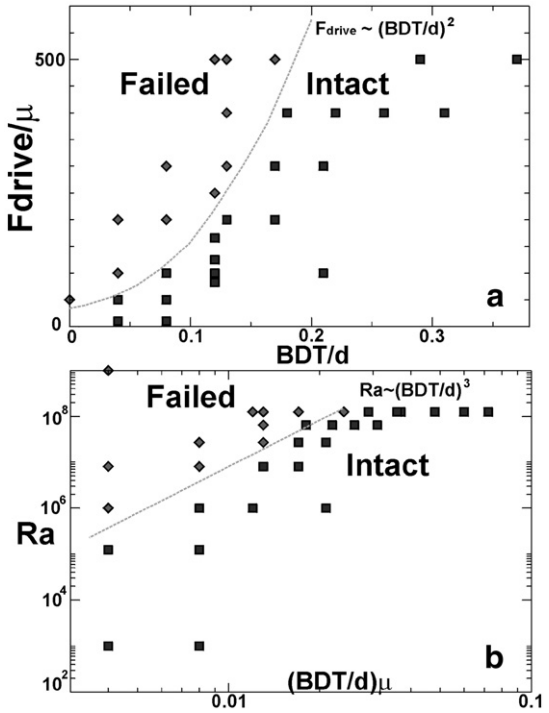

Fig. 3. (a) Linear plot of F_{drive}/μ vs BDT/d. Results of our simulations are also plotted. The transition between failed and intact lithosphere follows the relationship $F_{drive} \sim 33.73 + 1.4367 \times 10^4 (\mathrm{BDT}/d)^2$ for this $n=1$ case. (b) Log–log plot of Ra vs (BDT/d)μ. Calculation of Ra assumes the drip scaling discussed in the text. The transition between failed and intact lithosphere behaves as $Ra \sim 4.39 \times 10^{13} (\mu \mathrm{BDT}/d)^3$ for the $n=1$ case.

5×10^{21} Pas in all cases), and its thickness (assumed to scale with boundary layer thickness, ie. with d_{BDT}, see Section 3 and Table 2). These non-dimensional values were combined to derive F_{drive} (Section 2.3) and normalised d_{BDT}, as plotted in Fig. 4.

The largest uncertainty in F_{drive} is the use of an appropriate scaling exponent — a choice which is dictated by the dynamics (drip formation vs steady conduit flow or forced) and rheology (Newtonian vs non-Newtonian power-law rheology) of the system. The variation expected by using alternative scalings is encapsulated in the vertical size of the coloured regions in Fig. 4 (note the log scale).

The brittle–ductile transition for planets is calculated from estimates of their elastic lithospheric thickness (T_e), the relationship between the two is discussed in Maggi et al. (2000). T_e estimates depend strongly on the local rigidity and thermal boundary thickness, and vary considerably for a given planet. The elastic lithosphere for old oceanic lithosphere on Earth is ~40 km (Calmant et al., 1990; Watts and Burov, 2003; Jellinek and Manga, 2004; McNutt, 2004). For other planets and moons, we have adopted representative values from the literature (Table 2), and the width of the uncertainty regions in Fig. 4 include the variance in estimates of elastic thickness for these bodies. The coloured circles in Fig. 4 indicate bodies for which we only have a present-day estimate of τ_{drive} (the Galilean satellites). For the terrestrial planets, we have calculated how Ra (and hence F_{drive}), and TBL thickness (hence d_{BDT}) vary through time (see Table 2), and plotted their respective evolution from 4.5 Ga to present (black dots connected by arrows). An important caveat to these results is that we are not modelling plate tectonics, but establishing a minimum condition for this regime of mantle convection. We have used a fairly simplistic rheology and parameterization for the effective lithospheric strength, and more complex rheologies will complicate the picture. But the fundamental criterion, that mantle-generated stresses must be sufficient to overcome the effective lithospheric yield stress, is a condition that must be satisfied as a prerequisite for lid mobilisation and thus plate tectonics.

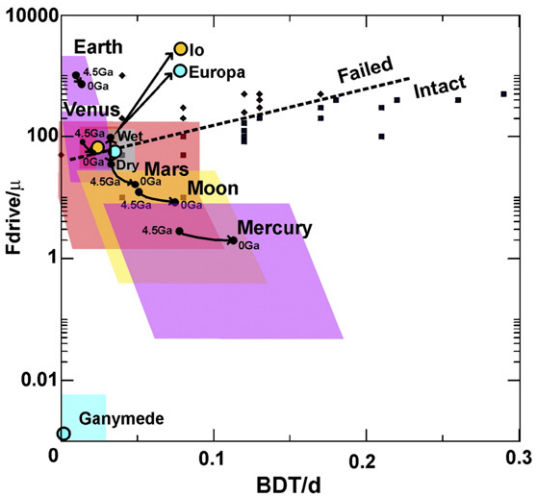

Fig. 4. Log-linear plot of the variation in tectonic style with increasing driving motive and depth to the brittle–ductile transition (BDT). The results of our numerical experiments are shown depending on their deformational response; blue squares indicate intact lithosphere, and red diamonds indicate failed lithosphere. The transition between the two regimes is plotted as a dashed line. Planets and satellites for which reliable estimates of mantle depth, elastic lithospheric thickness and mantle velocity exist (Table 2) are also non-dimensionalized and plotted. Driving forces at 4.5 Ga are determined assuming higher internal heat production and Rayleigh numbers (see Table 2). Coloured regions indicate the uncertainty in our estimates, based on the listed uncertainties in the elastic lithospheric thickness (Table 2), and the variance in the velocity scalings.

The primary difference between the Earth and Venus, as plotted in Fig. 4, is the existence of free water on the surface. This lowers the friction coefficient μ, and drastically reduces resistive strength of the lithosphere. The coefficient of friction is assumed to be 0.6 for dry rock (Kohlstedt et al., 1995), and 0.15 for rocky planets with free water on the surface (ie. Earth and early Mars). Free surface water results in the alteration of fault zones (specifically serpentinization of peridotite, Escartin et al. (1997)), and influences the pore pressure, which can reduce rock strength by on order of magnitude (Kohlstedt et al., 1995). The estimated maximum supportable stress from these results is in the vicinity of 40–150 MPa for Earth, depending on the scaling factors assumed, elastic lithospheric thickness, and effective coefficient of friction. If Venus has surface water at any time in its past, it could potentially have been in an active-lid mode of convection. Even without water, increased convective velocities, and lower T_e in the past suggest that Venus may have been in active-lid regime. Its position on the transition of the stagnant-lid regime today is consistent with the recent ($\sim$750 Ma) cessation of surface activity, and also permits the possibility of an episodic style of convection (Moresi and Solomatov, 1998; Turcotte, 1993). Episodic convection essentially involves long periods of quiescence — where the lid exhibits very little activity, interspersed by short periods of vigorous surface activity, where the lid is recycled in a massive pulse of fast, short-lived subduction (Moresi and Solomatov, 1998). In the context of Fig. 4, episodic convection can be thought of as an oscillation between the active and stagnant regimes. This oscillation occurs because of the time dependence of two competing factors: elastic lithospheric thickness and convective stress. After an overturn, the upper thermal boundary layer, and hence the elastic lithosphere, increases in thickness with time. At the same time the mantle, which was thoroughly cooled by the previous pulse of subduction, begins to heat up. Convection re-establishes itself (beneath the thickening lid) — and thus the internal velocities increase. However, at the same time, again due to increasing temperatures, the interior viscosities are similarly decreasing – and thus the time dependence of the induced convective stresses are themselves dependent on two competing factors (Eq. (1)) – the increasing internal velocities and decreasing viscosities after an overturn. Which of these effects wins out depends strongly on the rheology, and thermal configuration, of the system. For an episodic regime like that suggested for Venus, the re-establishment of convective velocities must dominate viscosity variations over the timescale considered, and thus the convective stresses of the system increase till they exceed the intrinsic strength of the lid, lid failure and a rapid pulse of subduction ensues, and the cycle repeats.

While Mars is probably in a stagnant regime now, and has been for much of its history, higher convective velocities, thinner thermal boundary layers, and the existence of surface water at 4 Ga (Catling, 2004) potentially place Mars in the active-lid regime of Fig. 3. We include the effect of free water by modifying the coefficient of friction to $\sim$0.15. Crustal magnetization in the Southern Highlands (Acuna et al., 1999) requires the existence of a dynamo on early Mars (Nimmo and Stevenson, 2000), suggesting plate-tectonics in early Martian history (Sleep, 1994; Lenardic et al., 2004), and our analysis suggests this is plausible. In contrast, there is no evidence of surface water on the Moon (Lissauer, 1997) or Mercury (Lewis, 1988), and both are predicted to have been stagnant for their entire history.

Io is the most volcanically active body in the solar system as a result of severe tidal heating from Jupiter. In fact, its predominant mode of heat loss is by volcanic resurfacing, and so it is clearly not in the "classic" stagnant lid mode of most other terrestrial planets, and such scalings are not directly applicable to it to derive interior velocities. However, the resurfacing rate of Io (McKinnon et al., 2000) places a constraint on interior velocities, and estimates of this plot Io on the transition between active and stagnant lid regimes, suggesting that non-volcanic surface tectonism is possible. Identification of rugged non-volcanic mountains (Carr et al., 1998) on Io indeed suggest that this deformational style is plausible. These rugged mountain ranges cover $\sim$2% of Io's surface, and show evidence of uplift and thrusting not directly related to Io's voluminous volcanism (Carr et al., 1998). One hypothesis for their formation is that they are tilted tectonic blocks, and that the tilting is in response to far-field volcanic loading and subsidence. In this case the body forces or "driving stress" is volcanic loading rather than a convecting rheological sublayer, but an analysis of driving versus resisting stresses is still possible — and such a comparison in Fig. 4 places Io on the borderline of having an active lid. This raises an important point, namely that lid-activity need not correspond to plate tectonics, and lid-failure and recycling can efficiently cool a planet with alternative tectonic regimes, as evidenced by Io. Io's geological evolution is not solely volcanic; the lid's response to stress is an important component of Io's current tectonic regime. A more detailed analysis of the body forces and non-volcanic tectonism on Io is difficult and not constrained by observations, as the stratification of tidal heating on Io is not well constrained (McKinnon et al., 2000; Carr et al., 1998; Moore, 2003), and structural styles are largely obscured by voluminous ongoing volcanism.

Similarly, assuming large strain-rate estimates for Europa (Ojakangas and Stevenson, 1989) constrain interior velocities, then the surface tectonic activity observed may have an intrinsic endogenic component, separate to tidally-induced cracking (Nimmo and Gaidos, 2002). Greenberg (2004) recently summarised the evidence for convergent features on Europa — which strongly suggests interior convective motions are having a discernible effect on the surface. Figueredo and Greeley (2004) argue that based on the lack on cross-cut impact craters, that the bulk of Europa's surface is very young (30–80 Myr). They suggest that the bulk of the ridge plains formed by a massive burst of activity and tectonic resurfacing 50–80 Myr ago, and that since then the regime has switched to a far more subdued cryovolcanic-dominated one. This is also consistent with the evolution in the width and linearity of observed bands, and consequently the inferred thickening of the elastic lithosphere (and cryosphere) over time. Based on our results, and its lithospheric history, we suggest that Europa may in fact be in an episodic regime similar to Venus. This would explain the massive resurfacing observed 50–80 Myr ago (Figueredo and Greeley, 2004), its more subdued surface activity since, and the gradual thickening of the lithosphere with time — and it is predicted by Fig. 4.

In contrast, despite having a relatively small elastic lithosphere, the extremely small estimated strain rates estimated for icy shell of Ganymede (Dombard and Mckinnon, 2001) preclude any surface deformation other than tidally-induced tectonic features.

5. Conclusion

We have shown that the driving force required to break an intact plate is a function of the depth to the brittle–ductile transition. Exceeding this critical driving force is a necessary condition for plate tectonics on terrestrial planets, and one that is met on the Earth. Less vigorous convection and thick elastic lithospheres preclude wholesale lid failure on smaller, colder planetary bodies, such as the Moon, Mercury, Ganymede, and present day Mars. On early Mars, more vigorous convective velocities, a thinner elastic lithosphere and the presence of free water on the surface could have resulted in plate tectonics. While the convective velocities and driving forces on Earth are intrinsically greater than for Venus, the first order difference between the two planets is surface water. Viscosity variations aside, our scalings predict that Venus may have been in an active-lid regime in the past due to increased convective velocities or if it possessed liquid water on its surface (Catling, 2004). Europa and Io both lay very close to the transition between active and stagnant lids — suggesting the possibility of tectonic resurfacing on these bodies, or at least a convective contribution to surface deformational features, such as the rugged non-volcanic mountains of Io, or convergent features on Europa.

Acknowledgements

This work was supported by NASA-MDAT grant NAG5-12166 and NSF Grant EAR-0448871. MJ acknowledges the assistance of the NSERC and The Canadian Institute for Advanced Research. This is GEMOC paper 484.

Appendix A. Convergence tests

We have run a simple convergent test for grid resolution for the model shown in Fig. 2a, and described in Sections 2 and 3. We have plotted the surface velocity field, once the model achieved a statistical steady state, against increasing grid resolution (Fig. A1). Our results demonstrate convergence towards a final result as resolution increases. A resolution of 128×64 elements is sufficient for a reliable accurate solution, increasing the resolution to 256×128 only marginally increases the accuracy.

Appendix B. Elasticity

We adopt a Maxwell viscoelastic model (more fully described in Moresi et al. (2003)). In this formulation, the deviatoric strain rate tensor $\hat{D}$ is assumed to be the sum of the elastic and viscous strain rate tensors, $\hat{D}_e$ and $\hat{D}_v$.

$$\frac{\overset{\nabla}{\tau}}{2G} + \frac{\tau}{2\eta_s} = \hat{D}_v + \hat{D}_e = \hat{D}. \tag{A1}$$

Here τ is the stress tensor, G is the shear modulus, and η_s is the shear viscosity. We incorporate the Jaumann corotational stress rate, $\overset{\nabla}{\tau}$, for a material point, to maintain mechanical objectivity. This is given by

$$\overset{\nabla}{\tau} = \dot{\tau} + \tau W - W\tau \tag{A2}$$

where W is the spin tensor,

$$W_{ij} = \frac{1}{2}\left(\frac{\partial V_i}{\partial x_j} - \frac{\partial V_j}{\partial x_i}\right). \tag{A3}$$

The importance of elasticity to our results can be assessed through a number of arguments.

1) For a shear modulus G of 5×10^{10}, and a viscosity η_s of 1×10^{22}, then the Maxwell time (η_s/G) is 6341 yr. In comparison, the time it takes a fast slab (velocity

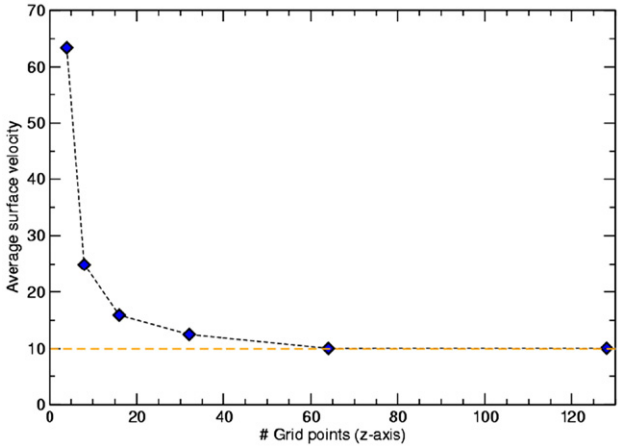

Fig. A1. Increased grid resolution (*x*-axis) against average steady-state surface velocities. The solution converges for higher resolutions.

5 mm/yr) to get through the bending zone of a trench (+/−350 km of the trench position (Turcotte and Schubert, 2002) is around 13.4 Myr. Thus viscous relaxation happens much faster than material advects through the bending zone, for realistic bulk lithospheric viscosities (Turcotte and Schubert, 2002).

2) Elasticity may focus lithospheric stresses (to the top and bottom edges of an elastic plate (Turcotte and Schubert, 2002)). For an elastic lithosphere of thickness T_e, the surface bending stress is given by $\tau = \frac{E}{1-\upsilon^2}\frac{(T_e/2)}{R}$, where here E is Young's modulus ($\sim 5\times10^{10}$), ν is Poisson's ratio ($\sim$0.25), and R is the radius of curvature (Turcotte and Schubert, 2002). Assuming, for example, an elastic lithospheric thickness of 30 km, and a radius of curvature of 300 km (typical scale of elastic behaviour around a subduction zone) then the maximum bending stress is 2.67 Ga — far in excess of the yield strength of the lithosphere. Conversely, assuming a typical yield strength of $\sim$30 MPa, the critical curvature to be *below* the yield stress is 26,667 km (ie. far in excess the radius of Earth). This implies that for any realistic curvature of the lithosphere, stress amplification will result in failure of the surface layers. A similar result can be found by applying the von Mises criterion for a viscoelastic material (Chapter 7 of (Turcotte and Schubert, 2002)).

3) For our argument, we are concerned with the maximum supportable lithospheric stress, which, as shown by Kohlstedt et al. (1995), occurs near the brittle–ductile transition. An elastic plate bends around its centre (the elastic core), such that while stress amplification may occur at the top and bottom surfaces, the stress amplification in the elastic core is zero. However, the lithosphere is not a free plate, and contains a substantial viscous component beneath its elastic layer, which tends to translate the deformational "core" to lower depths in the lithosphere. If the elastic core of the lithosphere approaches the brittle–ductile transition, then stress amplification in the strongest portion of the lithosphere is negligible.

Finally, we have run some tests of the sensitivity of our defined transition to variation in elastic parameters

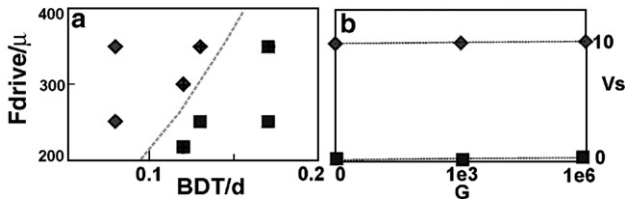

Fig. A2. a) Zoom-in of Fig. 4, illustrating points near the transition (crosses) where we tested the sensitivity of the transition to elastic parameters (by varying the shear modulus from 0 → 1e3 → 1e6). No effect on the position of the transition was noted. b) Variation in average steady-state surface velocity with increasing shear modulus. Variable shear moduli had little effect on this forced convection setup. Diamonds are for an active lid (Fig. 2a), squares are for an immobile lid (Fig. 2b).

(Fig. A2). We do not vary the geometry of the simulations. For large variations in our (non-dimensional) shear modulus, there was no discernible effect on the nature of the stagnant–active transition. Thus, while this promises to be an interesting avenue for future research, our analysis suggests that for a constant geometry, variations in elastic parameters is of 2nd order importance compared to variations in the yield strength of the plate in defining the stagnant–active-lid transition.

References

Acuna, M.H., Connerney, J.E.P., Ness, N.F., Lin, R.P., Mitchell, D., Carlson, C.W., McFadden, J., Anderson, K.A., Reme, H., Mazelle, C., Vignes, D., Wasilewski, P., Cloutier, P., 1999. Global distribution of crustal magnetization discovered by the Mars Global Surveyor MAG/ER Experiment. Science 284, 790–793.

Anderson, J.D., Lau, E.L., Sjogren, W.L., Schubert, G., Moore, W.B., 1996. Gravitational constraints on the internal structure of Ganymede. Nature 384, 541–543.

Anderson, J.D., Schubert, G., Jacobson, R.A., Lau, E.L., Moore, W.B., Sjogren, W.L., 1998. Europa's differentiated internal structure: inferences from four Galileo encounters. Science 281, 2019–2022.

Aoshima, C., Namiki, N., 2001. Structures beneath Lunar Basins, Estimates of Moho and elastic thickness from local analysis of gravity and topography. 32nd Annual LPSC Extended Abstracts, no.1561, Houston, Texas.

Batchelor, G.K., 1954. Heat convection and buoyancy effects in fluids. Q. J. R. Meteorol. Soc. 80, 339–358.

Beaumont, C., Hamilton, J., Fullsack, P., Muñoz, J.A., 2000. Factors controlling the Alpine evolution of the central Pyrenees inferred from a comparison of observations and geodynamical models. J. Geophys. Res. 105, 8121–8145.

Beeman, M., Durham, W.B., Kirby, S.H., 1988. Friction of ice. J. Geophys. Res. 93, 7625–7633.

Bird, P., Kong, X.H., 1994. Computer simulations of California tectonics confirm very low strength of major faults. Geol. Soc. Amer. Bull. 106, 159–174.

Byerlee, J.D., 1968. Brittle–ductile transition in rocks. J. Geophys. Res. 73, 4741–4750.

Calmant, S., Francheteau, J., Cazenave, A., 1990. Elastic layer thickening with age of the oceanic lithosphere: a tool for the prediction of the ages of volcanoes or oceanic crust. Geophys. J. Int. 100, 59–67.

Carr, M.H., McEwen, A.S., Howard, K.A., Chuang, F.C., Thomas, P., Schuster, P., Oberst, J., Neukum, G., Schubert, G., 1998. Mountains and Calderas on Io: possible implications for lithospheric structure and magma generation. Icarus 135, 146–165.

Catling, D.C., 2004. On Earth, as it is on Mars? Nature 429, 707–708.

Dombard, A.J., McKinnon, W.B., 2001. Formation of grooved terrain on Ganymede: extensional instability mediated by cold, superplastic creep. Icarus 154, 321–336.

Escartin, J., Hirth, G., Evans, B., 1997. Effects of serpentinization on the lithospheric strength and the style of normal faulting at slow-spreading ridges. Earth Planet. Sci. Lett. 151, 181–189.

Escartin, J., Hirth, G., Evans, B., 2001. Strength of slightly serpentinized peridotites: implications for the tectonics of oceanic lithosphere. Geology 29, 1023–1026.

Figueredo, P.H., Greeley, R., 2004. Resurfacing history of Europa from pole-to-pole geological mapping. Icarus 167, 287–312.

Folkner, W.M., Yoder, C.F., Yuan, D.N., Standish, E.M., Preston, R.A., 1997. Interior structure and seasonal mass redistribution of Mars from radio tracking of Mars Pathfinder. Science 278, 1749–1752.

Gordon, R.G., 2000. Diffuse oceanic plate boundaries: strain rates, vertically averaged rheology, and comparisons with narrow plate boundaries and stable plate interiors. In: Richard, M.A., Gordon, R.G., Van der Hilst, R.D. (Eds.), History and Dynamics of *Global Plate Motions*. Geophysical Monograph, vol. 121. American Geophysical Union, Washington DC, pp. 143–159.

Greenberg, R., 2004. The evil twin of Agenor: tectonic convergence on Europa. Icarus 167, 313–319.

Jellinek, A.M., Manga, M., 2004. Links between long-lived hotspots, mantle plumes, D" and plate tectonics. Rev. Geophys. 42. doi:10.1029/2003RG000144.

Jellinek, A.M., Lenardic, A., Manga, M., 2002. The influence of interior mantle temperature on the structure of plumes — heads for Venus, tails for Earth. Geophys. Res. Lett. 29 (1532). doi:10.1029/2001GL014624.

Jellinek, A.M., Gordon, R.G., Zatman, S., 2006. Experimental test of simple models of oceanic intraplate deformation. Geophys. J. Int. 164, 624–632.

Kaminski, E., Jaupart, C., 2003. Laminar starting plumes in high-Prandtl-number fluids. J. Fluid Mech. 478, 287–298.

Kanamori, H., 1994. Mechanics of earthquakes. Annu. Rev. Earth Planet. Sci. 22, 207–237.

Kohlstedt, D.L., Evans, B., Mackwell, S.J., 1995. Strength of the lithosphere: constraints imposed by laboratory experiments. J. Geophys. Res. 100, 17587–17602.

Konopliv, A.S., Binder, A.B., Hood, L.L., Kucinskas, A.B., Sjogren, W.L., Williams, J.G., 1998. Improved gravity field of the moon from Lunar Prospector. Science 281, 1476–1480.

Lenardic, A., Nimmo, F., Moresi, L., 2004. Growth of the hemispheric dichotomy and the cessation of plate tectonics on Mars. J. Geophys. Res. 109. doi:10.1029/2003JE002172.

Lewis, J.S., 1988. Origin and composition of Mercury. In: Vilas, F., et al. (Eds.), Mercury. Univ. Ariz. Press, Tuscon, Az, pp. 651–666.

Lissauer, J.J., 1997. Its not easy to make the Moon. Nature 389, 327–328.

Maggi, A., Jacson, J.A., McKenzie, D., Priestley, K., 2000. Earthquake focal depths, effective elastic thickness, and the strength of the continental lithosphere. Geology 28, 495–498.

Manga, M.D., Weeraratne, D., Morris, S.J.S., 2001. Boundary-layer thickness and instabilities in Bénard convection of a liquid with a temperature-dependent viscosity. Phys. Fluids 13, 802–805.

McGovern, P.J., Solomon, S.C., Smith, D.E., Zuber, M.T., Simons, M., Wieczorek, M.A., Phillips, R.J., Neumann, G.A., Aharonson, O., Head, J.W., 2002. Localized gravity/topography admittance and correlation spectra on Mars: implications for regional and global evolution. J. Geophys. Res. 107. doi:10.1029/2002JE001854.

McKinnon, W.B., Schenk, P.M., Dombard, A.J., 2000. Chaos on Io: a model for formation of mountain blocks by crustal heating, melting and tilting. Geology 29, 103–106.

McNutt, M., 2004. Lithospheric flexure and thermal anomalies. J. Geophys. Res. 89, 180–194.

Melosh, H.J., 1977. Global tectonics of a despun planet. Icarus 31, 221–243.

Moore, W.B., 2003. Tidal heating and convection on Io. J. Geophys. Res. 108. doi:10.1029/2002JE001943.

Moresi, L., Solomatov, V.S., 1995. Numerical investigation of 2D convection with extremely large viscosity variations. Phys. Fluids 7, 2154–2162.

Moresi, L., Solomatov, V., 1998. Mantle convection with a brittle lithosphere: thoughts on the global tectonic styles of the Earth and Venus. Geophys. J. Int. 133, 669–682.

Moresi, L., Dufour, F., Muhlhaus, H.-B., 2003. A Lagrangian integration point finite element method for large deformation modeling of viscoelastic geomaterials. J. Comp. Physiol. 184, 476–497.

Nimmo, F., Gaidos, E., 2002. Strike–slip motion and double ridge formation on Europa. J. Geophys. Res. 107. doi:10.1029/2000JE1476.

Nimmo, F., Stevenson, D.J., 2000. Influence of early plate tectonics on the thermal evolution and magnetic field of Mars. J. Geophys. Res. 105, 11969–11980.

Nimmo, F., Pappalardo, R.T., Giese, B., 2002. Effective elastic thickness and heat flux estimates on Ganymede. Geophys. Res. Lett. 29. doi:10.1029/2001GL013976.

Nimmo, F., Giese, B., Pappalardo, R.T., 2003. Estimates of Europa's ice shell thickness from elastically-supported topography. Geophys. Res. Lett. 30. doi:10.1029/2002GL016660.

Ogawa, M., Schubert, G., Zebib, A., 1991. Numerical simulations of three-dimensional thermal convection in a fluid with strongly temperature-dependent viscosity. J. Fluid Mech. 233, 299–328.

Ojakangas, G.W., Stevenson, D.J., 1989. Thermal state of an ice shell on Europa. Icarus 81, 220–241.

Reese, C.C., Solomatov, V.S., Moresi, L., 1998. Heat transport efficiency for stagnant lid convection with dislocation viscosity: application to Mars and Venus. J. Geophys. Res. 103, 13643–13657.

Schubert, G., Turcotte, D.L., Olsen, P., 2001. Mantle Convection in the Earth and Planets. Cambridge University Press, Cambridge, UK. 956 pp.

Segatz, M., Spohn, T., Ross, M.N., Schubert, G., 1988. Tidal dissipation, surface heat flow, and figure of viscoelastic models of Io. Icarus 75, 187–206.

Siegfried II, R.W., Solomon, S.C., 1974. Mercury: internal structure and thermal evolution. Icarus 23, 192–205.

Sleep, N.H., 1994. Martian plate tectonics. J. Geophys. Res. 99, 5639–5655.

Smrekar, S.E., Stofan, E.R., 2003. Effects of lithospheric properties on the formation of Type 2 coronae on Venus. J. Geophys. Res. 108. doi:10.1029/2002JE001930 (Assuming largest Te, to eliminate thermal and rifting effects).

Solomatov, V.S., 2004a. Initiation of subduction by small-scale convection. J. Geophys. Res. 109. doi:10.1029/2003JB002628.

Solomatov, V.S., 2004b. Correction to "Initiation of subduction by small-scale convection". J. Geophys. Res. 109. doi:10.1029/2004JB003143.

Solomatov, V.S., Moresi, L., 1997. Three regimes of mantle convection with non-Newtonian viscosity and stagnant lid convection on the terrestrial planets. Geophys. Res. Lett. 24, 1907–1910.

Solomatov, V.S., Moresi, L., 2000. Scaling of time-dependent stagnant lid convection: application to small-scale convection on Earth and other terrestrial planets. J. Geophys. Res. 105, 21795–21818.

Tozer, D.C., 1972. The present thermal state of the terrestrial planets. Phys. Earth Planet. Inter. 6, 182–197.

Turcotte, D.L., 1993. An episodic hypothesis for Venusian tectonics. J. Geophys. Res. 98, 17061–17068.

Turcotte, D.L., Schubert, G., 2002. Geodynamics. Cambridge University Press, Cambridge, New York. 450 pp.

Watts, A.B., Burov, E.B., 2003. Lithospheric strength and its relationship to the elastic and seismogenic layer thickness. Earth Planet. Sci. Lett. 213, 113–131.

Worster, M.G., Leitch, A.M., 1985. Laminar free convection in confined regions. J. Fluid Mech. 156, 301–319.